JOURNAL OF GEOPHYSICAL RESEARCH, VOL. 112, E04003, doi:10.1029/2006JE002826, 2007

Olympus Mons, Mars: Inferred changes in late Amazonian aged effusive activity from lava flow mapping of Mars Express High Resolution Stereo Camera data

Jacob E. Bleacher,[1,2] Ronald Greeley,[1] David A. Williams,[1] Stephanie C. Werner,[3] Ernst Hauber,[4] and Gerhard Neukum[3]

Received 9 September 2006; revised 15 November 2006; accepted 8 December 2006; published 18 April 2007.

[1] Lava flow mapping was conducted on a north-south transect of Olympus Mons using the European Space Agency's Mars Express High Resolution Stereo Camera (HRSC) image H0037. The HRSC image was coregistered to Mars Orbiter Laser Altimeter, Thermal Emission Imaging System, and Mars Orbiter Camera data, enabling lava flow structures to be differentiated and mapped consistently across the shield. Because different structures develop as a result of different effusive conditions, their abundance and distribution provide insight into the eruptive history of a shield volcano. Results show that lava channels are the dominant flow structure, whereas tabular sheets are most common beyond the basal scarp. A hummocky unit dominates the summit area and likely represents a combination of (1) volcanic lava flows, (2) pyroclastic deposits, (3) a dust mantle, and (4) frozen volatiles, all of which have been suggested to exist on Olympus Mons in the past. Lava fans are typically associated with lava tubes, indicating that they represent tube outbreaks as was previously suggested as one possible formation mechanism. No vents were identified, suggesting that major rift zones have not developed on the north or south flank. Younger channel-fed flows typically embay older tube-related flows, which they outnumber by a ratio of 5:1. Therefore Olympus Mons likely experienced a change in eruptive style from longer-lived, stable, tube-forming eruptions to shorter-lived, less stable, channel-forming eruptions in the late Amazonian. A similar trend exists for the Hawaiian volcanoes in which a decrease in the magma production rate drives a change to dominantly channel forming eruptions associated with increased shield age.

Citation: Bleacher, J. E., R. Greeley, D. A. Williams, S. C. Werner, E. Hauber, and G. Neukum (2007), Olympus Mons, Mars: Inferred changes in late Amazonian aged effusive activity from lava flow mapping of Mars Express High Resolution Stereo Camera data, *J. Geophys. Res.*, *112*, E04003, doi:10.1029/2006JE002826.

1. Introduction

[2] The Martian volcano Olympus Mons is the highest and most prominent shield volcano in the solar system, with a height of ~22 km and a width of ~640 km based on Mars Orbiter Laser Altimeter (MOLA) data [*Smith et al.*, 2001; *Plescia*, 2004]. Its location at 19°N, 225°E suggests a genetic link to the Tharsis province [*Smith et al.*, 1999]. Because of limitations in data resolution, geologic maps of Olympus Mons do not consistently differentiate lava flows by emplacement style (i.e., channel fed versus tube fed). This distinction is important when interpreting the effusive history of a shield volcano as different lava flow structures typically develop as a result of different eruption conditions, lava properties, and planetary variables [*Greeley*, 1977; *Head et al.*, 1981; *Whitford-Stark*, 1982]. For this reason, an understanding of the abundance and distribution of different lava flow types serves as a geologic framework for understanding basaltic volcanic systems [*Head et al.*, 1981]. Because this framework has not yet been established for Olympus Mons, details of its most recent effusive activity and possible links to the Tharsis province remain elusive.

[3] New insight into the eruptive evolution of Olympus Mons can be obtained by mapping on high-resolution images. The systematic characterization of surface lava flows and their distribution in time and space is essential for identifying any evolution in the volcanic processes working on and within the volcano. Thus the objective of this work was to investigate the most recent effusive activity at Olympus Mons by mapping different lava flow types and characterizing their stratigraphic relationships and distributions. We used Mars Express (MEX) High Resolution Stereo Camera (HRSC) [*Neukum et al.*, 2004a] data that

[1]School of Earth and Space Exploration, Arizona State University, Tempe, Arizona, USA.
[2]Now at Planetary and Geodynamics Laboratory, NASA Goddard Space Flight Center, Greenbelt, Maryland, USA.
[3]Institute of Geological Sciences, Freie Universitaet, Berlin, Germany.
[4]Institute of Planetary Research, German Aerospace Center, Berlin, Germany.

0148-0227/07/2006JE002826$09.00

are geometrically rectified to the Mars Global Surveyor (MGS) MOLA 128 pixel/degree gridded data record [*Smith et al.*, 2003] as our map base providing regional coverage at high resolution. These data are supplemented with MGS Mars Orbiter Camera (MOC) [*Malin et al.*, 1992; *Malin and Edgett*, 2001] data, which provide higher resolution over specific sites, and Mars Odyssey (MO) Thermal Emission Imaging System (THEMIS) [*Christensen et al.*, 2004] data, which provide images with additional illumination angles at comparable resolution to HRSC.

2. Background

[4] Olympus Mons was first recognized as a shield volcano on the basis of morphological similarities to Hawaiian shields in 1972–1974 Mariner 9 orbiter images [*McCauley et al.*, 1972]. Early Viking-based maps show Olympus Mons as a large shield volcano consisting of a single unit of lightly cratered volcanic material in which the impact crater density indicated a late Amazonian age (<300 million years (Ma)) [*Scott and Carr*, 1978; *Plescia and Saunders*, 1979; *Hartmann et al.*, 1981; *Scott and Tanaka*, 1981a, 1981b; *Scott et al.*, 1981a, 1981b; *Scott and Tanaka*, 1986].

[5] *Morris and Tanaka* [1994] produced Viking-based geologic maps of the shield (at scales of 1:2,000,000 and 1:1,000,000) in which three nested units (Aos_1, Aos_2, and Aos_3) and a fourth, younger unit of pristine flows (Aos_4) were differentiated. Unit Aos_3 is described as narrow, leveed flows hundreds of meters to several kilometers wide and 10 to >100 km long, with indistinct beginnings and terminations in which radial ridges likely enclose lava tubes. Unit Aos_2 is described as flows with a rough, hummocky surface, containing tonque-like flows with leveed channels and broad sheets. Unit Aos_1 is described as flows with indistinct boundaries and hummocky surfaces containing irregular to round pit craters in chains or clusters.

[6] *Morris and Tanaka* [1994] showed the oldest unit (Aos_1) at the summit and the youngest unit (Aos_3) at the shield's base, indicating a decrease in age distally, with individual younger flows (Aos_4) emplaced over the other three units. *Carr et al.* [1977] suggested that the distal flows were erupted from vents near the summit and were emplaced via long distributary systems of tubes and channels. Lava flows of all four units cover large (tens of kilometers) terraces, likely formed as a result of large slip faults [*Thomas et al.*, 1990; *McGovern and Solomon*, 1993]. Lava fans are suggested to represent local outpourings of lava from buried tubes [*Carr et al.*, 1977], eruptive vents along deep concentric fractures [*Morris and Tanaka*, 1994], or vents fed by radial dikes [*Mouginis-Mark and Christensen*, 2005]. Lava flows embay and are truncated by a basal scarp with a height of up to 10 km [*McGovern et al.*, 2004]. Recent crater counts confirm a late Amazonian age for the flanks, indicating that it is one of the youngest volcanic features on Mars [*Neukum et al.*, 2004b; *Werner*, 2005; *Basilevsky et al.*, 2006].

[7] A key point about the mapping of Olympus Mons is that even the most recent mapping campaign [*Morris and Tanaka*, 1994] was limited to grouping different lava flow structures because of limitations in image resolution. This distinction is important because different structures form as a result of different eruption and emplacement conditions. Basaltic eruptions typically produce channels or tubes that deliver lava to the flow fronts [*Wentworth and Macdonald*, 1953; *Macdonald*, 1956]. Observations of active basaltic flows show that tubes tend to form during long-lived, stable eruptions of low-viscosity lavas at low to moderate effusion rates, whereas channels tend to develop during shorter-lived, unstable eruptions of higher-viscosity lavas at moderate to high effusion rates [*Greeley*, 1973; *Holcomb*, 1987; *Greeley*, 1987; *Rowland and Walker*, 1990; *Peterson et al.*, 1994; *Kauahikaua et al.*, 1998; *Heliker et al.*, 1998; *Calvari and Pinkerton*, 1998, 1999; *Calvari et al.*, 2003, *Kauahikaua et al.*, 2003, *Bailey et al.*, 2006]. Lava tubes generally extend lava flows because they typically result from longer-lived eruptions and they insulate the lava [*Swanson*, 1973; *Keszthelyi*, 1995; *Sakimoto and Zuber*, 1998].

[8] The relationship between eruptive conditions and morphology enabled researchers to determine that Kilauea has experienced longer-lived and more stable eruptions in the Holocene compared to Mauna Loa, which displays less tube-fed flows, as determined from mapping aimed at differentiating lava flow types [*Greeley*, 1987; *Holcomb*, 1987; *Lockwood and Lipman*, 1987]. Although geologic mapping of lava flows proved useful for improving the understanding of terrestrial basaltic systems [see also *Rowland*, 1996], a similar approach has not yet been rigorously applied to Martian shield volcanoes because of a lack of image data combining spatial resolution high enough to resolve different lava flow types over areas sufficiently large enough for consistent regional mapping. However, the acquisition of new image data (HRSC, THEMIS, and MOC) provides the unprecedented opportunity to characterize the latest effusive activity at Olympus Mons.

3. Methods

[9] HRSC image H0037 centrally transects Olympus Mons from north to south with a ~80 km wide image swath, at a resolution ranging between 16.5 and 20.5 m/pixel in the nadir channel, including two stereo channels (at half the nadir resolution) and four color channels (at one-fourth nadir resolution). Using the Video Image Communication and Retrieval (VICAR) software (http://www-mipl.jpl.nasa.gov/external/vicar.html), modified by the German Aerospace Center (DLR), we processed H0037 into a sinusoidal, orthographic projection with a central meridian of 225°E. We then processed THEMIS and MOC images with the Integrated Software for Imagers and Spectrometers (ISIS) software (http://isis.astrogeology.usgs.gov/index.html) into the same projection. We used ArcGIS 9.1 by Environmental Systems Research Institute Inc. (ESRI) to place the MOLA grid in a corresponding projection.

[10] Our mapping differentiated lava flow types to estimate their abundances (based on surface area) across the volcano (Figure 1). There are well-established criteria for identifying lava flow types on Olympus Mons [*Carr*, 1973; *Greeley*, 1973; *Carr et al.*, 1977; *Greeley and Spudis*, 1981; *Mouginis-Mark et al.*, 1992; *Morris and Tanaka*, 1994], as well as terrestrial volcanoes [*Carr and Greeley*, 1980; *Holcomb*, 1987; *Greeley*, 1987; *Rowland*, 1996]. We use these studies as our basis for consistently mapping lava tubes, leveed channels, raised flows lacking channels or skylights, sheets, or other previously unidentified units (Figure 2).

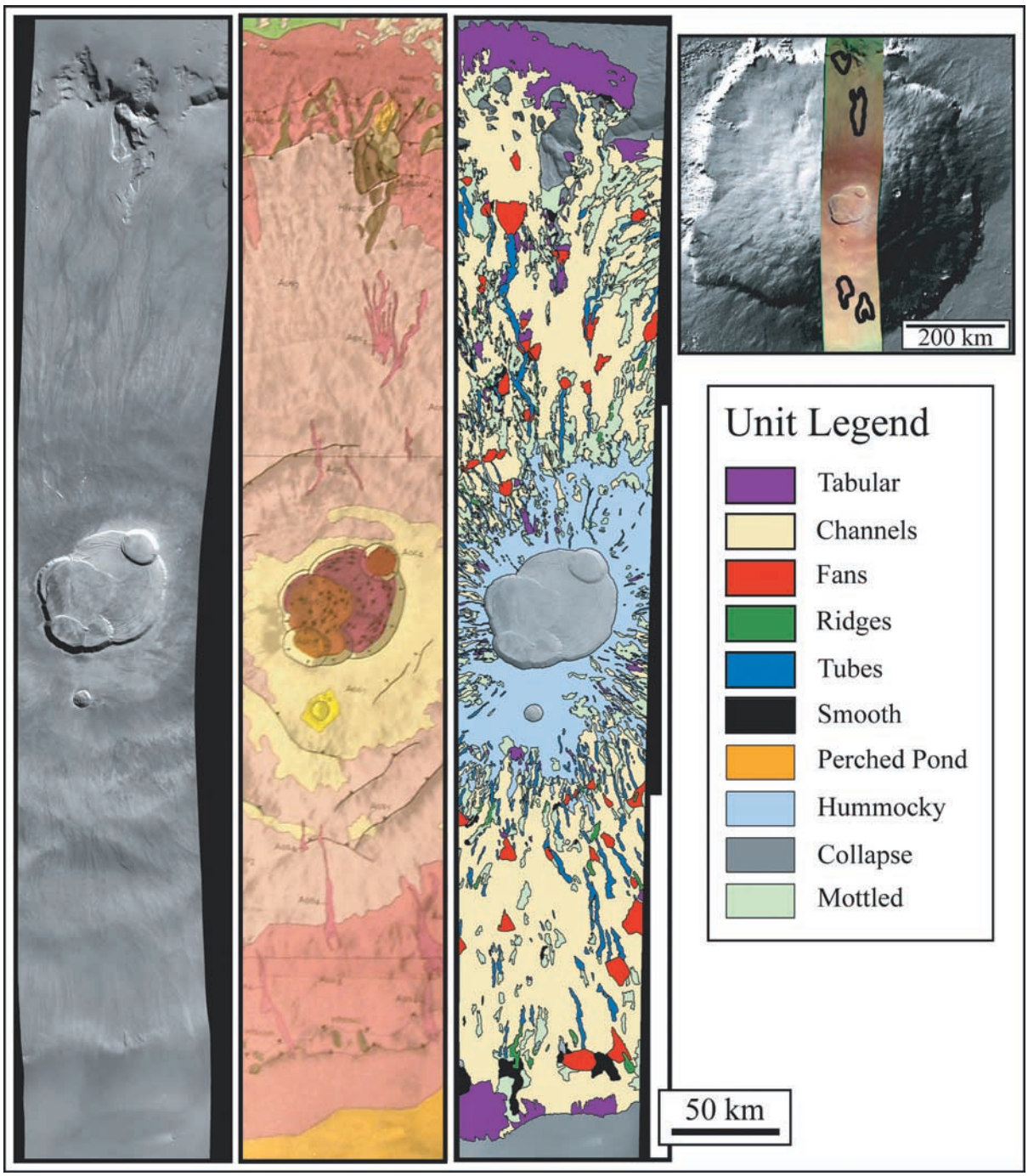

Figure 1. H0037 nadir image covering Olympus Mons is shown (left strip) along with a corresponding portion of the geologic map of *Morris and Tanaka* [1994] (middle strip) and our lava flow map (right strip). The type examples of lava flow map units named in the legend are shown in Figure 2. The HRSC color image strip from MEX orbit 37 is coregistered to MOLA and is shown as context at the top right. Areas for which crater counts were conducted are outlined in black on the HRSC color image.

[11] The GIS software enables derivation of slope [*Burrough and McDonell*, 1998; *Longley et al.*, 2001] from the MOLA data. This approach makes possible an assessment of relationships between the lava flows and the topography. We determined the median slope for the Olympus Mons flank and used it as the quantitative descriptor of the slope of the volcano as the median has been shown to best describe the typical slope of a landscape [*Kreslavsky and Head* 1999, 2000; J. E. Bleacher and R. Greeley, Relating volcano morphology to the developmental progression of Hawaiian shield volcanoes through slope frequency and hypsometric analyses of SRTM data, submitted to *Journal of Geophysical Research*, 2007, hereinafter referred to as Bleacher and Greeley, submitted manuscript, 2007].

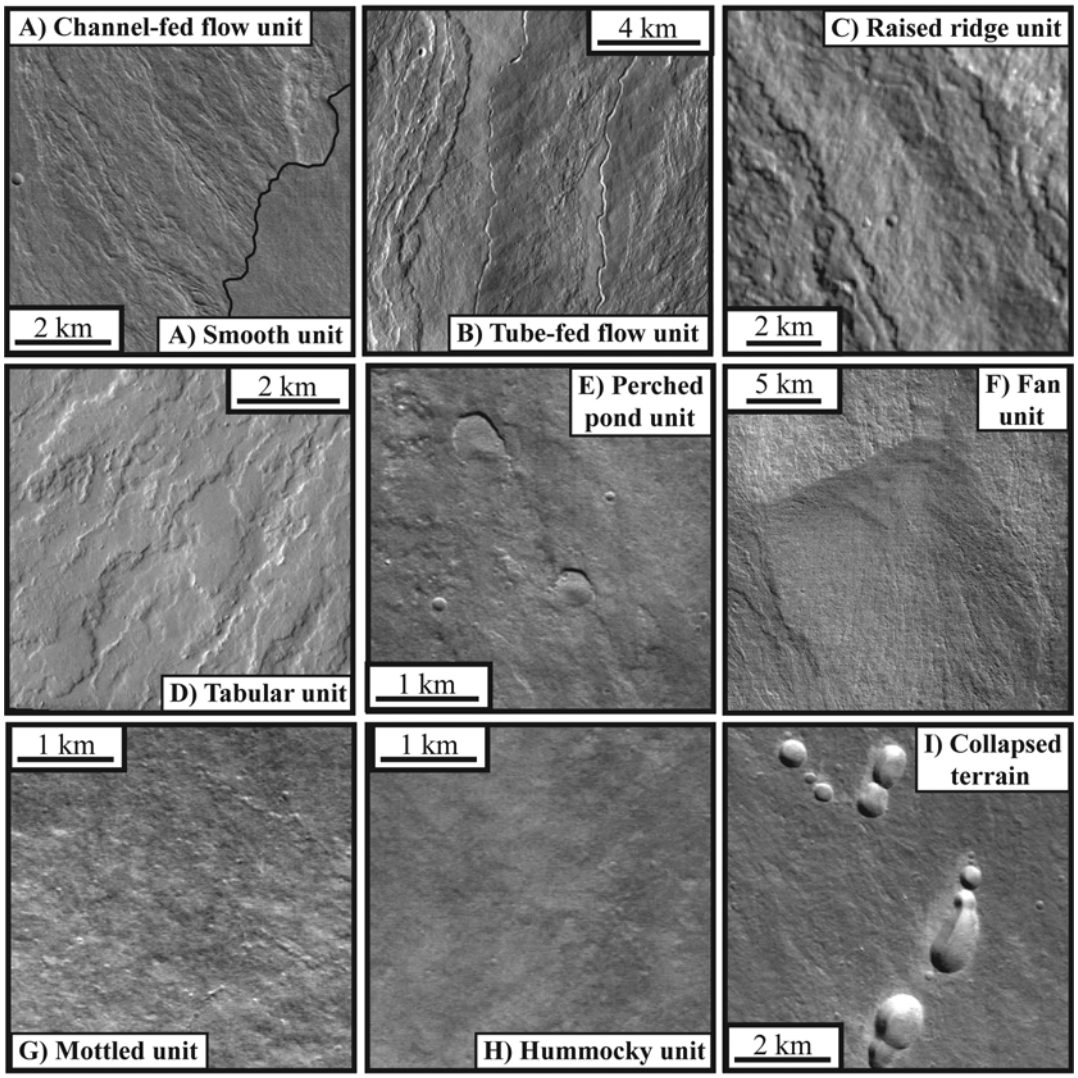

Figure 2. Type examples of map units named in Figure 1: (a) channel-fed flow unit and the smooth unit, (b) tube-fed flow unit, (c) raised ridge unit, (d) tabular unit, (e) perched pond unit, (f) fan unit, (g) mottled unit, (h) hummocky unit, and (i) collapsed terrain. Examples are taken from HRSC H0037 nadir image except for Figures 2b–2d, which are taken from THEMIS images V11326014, V16530005, and V11326016, respectively. North is to the top for each image, and solar illumination is from the bottom left.

[12] Superposition relationships and crater model ages provide insight into the eruptive sequence and possible evolution in effusive style. We determined crater retention ages for four channel-fed flow fields identified during mapping (Figure 1), on the basis of impact crater frequency distributions using the algorithm of *Hartmann and Neukum* [2001]. We conducted crater counts for areas of overlapping flows of similar morphology, providing an average age for different flow fields on each flank. Uncertainties and assumptions necessary for modeling surface ages from impact crater accumulation exist because of potential volcanic collapse depressions, other nonimpact depressions, modification by nonvolcanic processes, and secondary craters [*Greeley and Gault*, 1979; *Edgett and Malin*, 2002; *McEwen et al.*, 2005; *Plescia*, 2005]. However, the retention ages are used here as relative dating in coordination with superposition relationships [see *Hartmann*, 2005] to provide insight into the sequence of lava flow emplacement.

[13] To determine unit abundances, we normalized each unit's surface area to the total area of the mapping region. In order to quantify the distribution of flow types across the volcano we plotted normalized distance from the caldera against normalized flow abundance. To do so, we produced a window with a width equal to 5% of the total distance from the caldera to the distal extent of the Olympus Mons flows (~300–320 km). The normalized surface area within the window was calculated for each unit at intervals equal to 2.5% of the distance from the caldera to the distal margin of the shield. The result is a plot of the abundance of each lava flow type with respect to the position on the flank (Figure 3), enabling us to measure how each flow's abundance varies distally.

[14] We analyzed the results from lava flow mapping and age estimates for possible relationships to local topography.

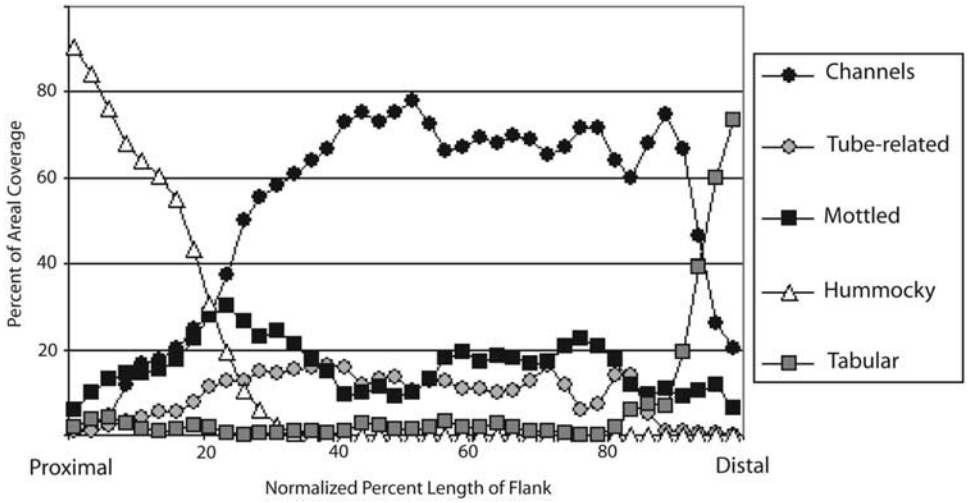

Figure 3. Plot showing the percent coverage of the most abundant units versus the normalized length of the flanks. Abundance values are calculated for an area equal in length to 5% the distance from the caldera to the distal margin. Area calculations were conducted at equal intervals spaced at 2.5% the distance from the caldera to the distal margin.

Of particular interest are potential associations between map units and slope that might provide insight into their formation. For example, terraces on the middle flanks are regions of increased slope [*Plescia*, 2004] that might be associated with changes in flow morphology. Both observational [*Guest et al.*, 1987; *Kilburn and Lopes*, 1991] and laboratory-based [*Gregg and Fink*, 2000] evidence supports this relationship on Earth. We integrated the distribution of flow types, their relations to topography, and relative ages and synthesized these data to identify trends that might be related to evolution of the volcano, as has been suggested for Martian volcanism in general [*Carr et al.*, 1977; *Crumpler and Aubele*, 1978; *Greeley and Spudis*, 1981; *Mouginis-Mark et al.*, 1992]. We compared the Olympus Mons results to analyses of the Hawaiian shields to identify any comparable trends that might provide insight into magma production and tectonic setting on Mars.

4. Results

4.1. Unit Descriptions

[15] Our map area is ~75,000 km^2, covering ~20% of Olympus Mons between 13° and 24°N and 226° and 228°E. We defined and characterized nine primary units, of which several were modified, resulting in an additional terrain, including the (1) channel-fed flow unit, (2) tube-fed flow unit, (3) raised ridge unit, (4) fan unit, (5) tabular unit, (6) perched pond unit, (7) mottled unit, (8) hummocky unit, (9) smooth unit, and (10) collapsed terrain (Figure 2). The caldera complex and tectonic blocks (generally restricted to the basal scarp) were excluded from our mapping. A ~12 km diameter crater ~20 km south of the caldera produced an ejecta blanket that has affected the nearby volcanic morphology. Although we were unable to identify a clear margin to the ejecta, we excluded a one crater diameter area surrounding the crater rim from the lava flow abundance calculations.

[16] The channel-fed flow unit is typified by subparallel linear channels often displaying levees (Figure 2a). This unit is inferred to be composed of individual channel-fed lava flows and larger channel-fed flow fields, as are often seen on terrestrial volcanoes. Individual channel-fed flow fields are not subdivided except when conducting crater counts. Within this study, individual channels could not be traced for more than several tens of kilometers, supporting the findings of *Basilevskaya et al.* [2006], as they tend to be covered by other flows. Some channels are truncated by the caldera, but the source region for nearly all other channel-fed flow fields is undetermined because of burial by younger flows. Although some individual flows are over 1 km wide, the typical flow width detected at this resolution is on the order of several hundred meters, as was also measured by *Basilevskaya et al.* [2006]. However, lava channels of smaller widths were seen using MOC data by *Malin and Edgett* [2001] and also within this study.

[17] The tube-fed flow unit (Figure 2b) displays sinuous chains of collapse pits, inferred to be skylights or partially collapsed lava tubes, sometimes gradational with a sinuous trench (i.e., completely collapsed tube roof) as is seen on Earth. Within this study the tube-fed flow unit includes a smooth to hilly terrain (at the tens to hundreds of meters horizontal scale) adjacent to the skylights and typically ranges up to several kilometers in width, while the skylights themselves were measured by *Pupysheva et al.* [2006] to typically be 130–270 m in width and 10–22 m in depth. Lengths are highly variable, with the longest flow field reaching ~60 km on the south flank and ~100 km on the north flank. Skylights are often axial to ridges that rise to ~100 m above the surrounding lava flows or on surfaces that lack any topographic expression. Tube-fed flows are typically embayed by younger flows.

[18] The raised ridge unit (Figure 2c) is similar to the tube-fed flow unit but lacks collapses. This unit consists of a sinuous to linear ridge or group of adjacent hills. Ridges have comparable widths and heights but are typically shorter in length (none longer than ~15–20 km) than tube-fed flows. The raised ridge unit is inferred to represent

Table 1. Abundances for Each Unit Within the Map Area as a Normalized Percent of the Total Surface Area of the Map and Each Flank

Map Unit	Full Map	North Flank	South Flank
Channels	50	47	56
Hummocky	17	12	17
Mottled	16	21	10
Tubes	5	4	6
Ridges	1	1	1
Fans	3	4	4
Tabular	8	10	5
Smooth	0	1	1
Collapses	0	0	0
Ponds	0	0	0

a lava tube or lava tube-fed flow field for which roof collapse has not occurred or is not detectable. The tabular unit (Figure 2d) displays a relatively smooth surface bound by lobate margins. This unit is inferred to be lava flows emplaced as sheets or the distal edge of channel- or tube-fed flows that cannot be linked to the channel- or tube-fed flow unit. Displaying a similar morphology to the tabular unit is the perched pond unit (Figure 2e), which shows a lobate margin and relatively smooth surface but for which the flow surface is topographically lower than the flow margin.

[19] The fan unit (Figure 2f) is composed of positive topographic, delta-like features, which in some cases diverted younger flows. The apex of an individual fan marks its highest topographic point and usually consists of one hill or a cluster of several hills from which a somewhat linear texture radiates downslope. Fan dimensions are highly variable and are often influenced by embayment from younger flows that obscure the true dimensions of the fans. The fans range from a few kilometers wide up to as large as ~20 km wide, in one example. The apex of some lava fans are up to 100 m higher than adjacent flows.

[20] The mottled unit (Figure 2g) is typified by a rough surface at a horizontal scale of tens to hundreds of meters displaying mounds inferred to be only a few meters high on the basis of MOC image analysis. Similar to the mottled unit is the hummocky unit, which has a hilly surface at the horizontal scale of a few kilometers (Figure 2h). Both the mottled and hummocky units lack clear margins and are often gradational with other units. The "smooth unit lacks flow margins and any clear surface texture (Figure 2a). Several units have been heavily modified creating a collapsed terrain (Figure 2i) that is typified by chains of ovoid depressions or smooth floored trenches. The collapses are generally a kilometer or greater in diameter, significantly larger than the collapsed tube roofs measured by *Pupysheva et al.* [2006], and they do not display raised rims. Therefore these features are not considered to represent lava tube roof collapse or impact events.

4.2. Unit Relationships and Ages

[21] The units mapped in this study display several relationships that are consistent across the volcano. The somewhat linear texture of the fan unit typically transitions to channel-fed flows distally from the apex. There are also several instances of the tube-fed flow and raised ridge units located within or trending out of a fan near the transition to channels. Tube-fed flows trend out of or into the apex of ~80% of the lava fans, while fans that lack this relationship with tubes are embayed by younger channel-fed flows that were diverted around the apex.

[22] The median slope of the shield is 3° when excluding the basal scarp. Flank terraces and the basal scarp typically display slopes between 6° and 10° and 15° and 40°, respectively. Nearly 40% of the lava fans are located along the base of flank terraces or the basal scarp, and nearly all fans are associated with slopes that are <2°. Therefore the fan unit is typically located on slopes lower than the shield median or typical of the terraces and basal scarp.

[23] The channel-fed flow unit also displays an embayment relationship with the typically older tube-fed flow and raised ridge units, often showing that their flow direction was controlled by the positive topography of the older flows. Relative to one another, tube-related flows decrease, while channel-fed flows increase in abundance distally. Two large channel-fed flow fields were identified on both the north and south flank for which crater counts were conducted. Crater retention ages and superposition relationships suggest that distal channel-fed flow fields are older than proximal fields.

4.3. Unit Abundances and Distributions

[24] Our HRSC-based mapping enables an assessment of the overall abundance (by surface area) of flow types and their distribution across Olympus Mons (Table 1). Within the map the channel-fed flow unit covers ~50% of the flank, whereas the tube-fed flow unit covers ~6%. The hummocky and mottled units cover 17 and 16%, respectively. All other units cover <10% of the flank, with the smooth and perched pond unit and the collapsed terrain representing <1% of the surface.

[25] The distribution of each unit with respect to the normalized percent distance from the caldera to the distal extent of the shield (~300 km) is shown in Figure 3. On the basis of morphology and unit relationships the tube-fed flow, raised ridge, and fan units are combined as tube-related, as will be discussed in section 5. Although the channel-fed flow unit is the most abundant, the summit is dominated by the hummocky unit to ~20% of the distance to the distal margin (matching well with the subdued Aos_1 unit of *Morris and Tanaka* [1994]). The hummocky unit transitions into a combination of channel-fed flow, tube-fed flow, and mottled units distally, and the channel-fed flow unit is dominant beyond 20% of the distance to the distal margin. The tabular unit is infrequently and randomly distributed across the flank but is the most common unit beyond ~95% distance to the distal margin. Tube-related and mottled units are dominantly located between 20 and 85% of the distance to the distal margin. The perched pond and smooth units and collapsed terrain are excluded from Figure 3 as their abundance is consistently <1% surface area. Both the perched pond unit and collapsed terrain are restricted to the summit.

5. Discussion

[26] Our mapping results provide new insight into the late Amazonian effusive history of Olympus Mons. The unit

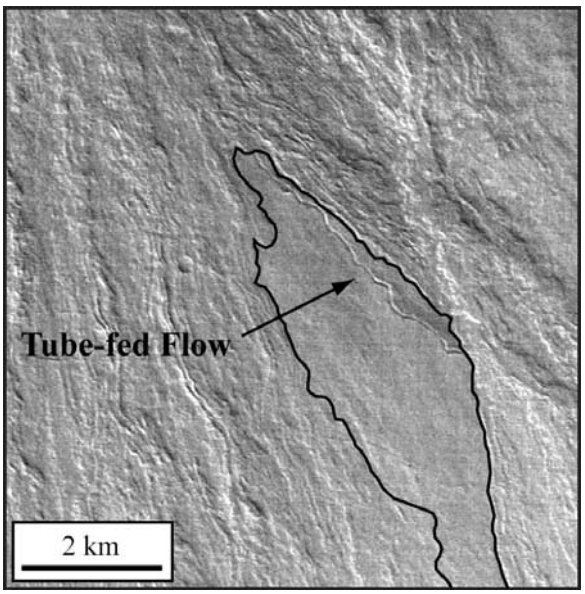

Figure 4. HRSC image H0037 showing the typical relationship between lava channels and tubes on Olympus Mons. Younger channel-fed flows embayed the older tube-fed flow. North is toward the top, and solar illumination is from the bottom left.

distributions show that the summit is dominated by the hummocky unit out to ~20% distance to the distal margin, where the channel-fed flow unit becomes dominant. At 95% distance to the distal margin a transition to the tabular unit being dominant occurs, beyond which the lava flows of Olympus Mons that make up the tabular unit in this area are embayed by Tharsis plains flows. The typical basal scarp slopes are 15°–40° and mark a transition from the 3° median slope on the main flank to <2° on the adjacent plains. On Earth, an increase in lava flow width is shown to occur in the distal regions and where slopes decrease [*Guest et al.*, 1987; *Kilburn and Lopes*, 1991; *Gregg and Fink*, 2000]. Because tabular lava flows in this area represent the distal flows and a transition to lower slopes, we suggest that these factors control the observed change in morphology.

[27] No obvious structural feature is related to the transition from the hummocky to channel-fed lava flow unit. *Holcomb* [1987] showed that the summit of Kilauea is dominated by surface-fed flows resulting from caldera spill over, in which major channels and tubes did not develop, potentially similar to the hummocky terrain. Elsewhere, pyroclastic deposits are suggested to cover large areas surrounding the Tharsis Montes, potentially producing a similar morphology to the hummocky unit here [*Edgett*, 1997; *Edgett et al.*, 1997; *Mouginis-Mark*, 2002]. Olympus Mons also displays evidence of a dust mantle [*Morris and Tanaka*, 1994; *Bandfield et al.*, 2000; *Mellon et al.*, 2000; *Malin and Edgett*, 2001], which if deposited during global storms, is likely to be thicker at higher elevations as the less dense atmosphere might not be able to reentrain the dust [*Greeley and Iversen*, 1985]. *Basilevsky et al.* [2005] describe a hummocky-like surface in the western basal scarp region, which they conclude is composed of frozen volatiles, fine-grained pyroclastics, and dust. On the basis of these observations we conclude that the hummocky unit surrounding the summit is a combination of (1) lava flows covered by (2) pyroclastic deposits, (3) dust, and (4) frozen volatiles. Continued analysis with higher-resolution instruments might better reveal the nature of the hummocky unit.

[28] The relationship between tubes and fans suggests that within our map area, fans represent local outpourings of lava resulting from impeded flow of lava within a tube, as originally suggested by *Carr et al.* [1977]. Tube outbreaks appear to be slope related (<2°) in some cases, similar to talus-and-lava cones described by *Holcomb et al.* [1974] at Hawaii, while tube outbreaks might also have resulted from temporary or permanent blockages by rafted, solidified lava. Fans are often morphologically upstream of distal channel-fed flow fields and many fans transition to lava channels distally from their apex. Therefore the fans appear to be a midflank source for many distal channel-fed flow fields, while the fans themselves appear to source from tube-fed flows, which can act as a surface extension of a volcano's conduit system [*Greeley*, 1987]. Although some fans do not show a direct link to lava tubes, those examples are also heavily embayed by younger channel-fed flows. Therefore we suggest that fans for which no link to lava tubes are observed were likely associated with a tube but that the observable link has subsequently been buried by younger lavas.

[29] If the hypothesis that all fans were linked to lava tubes (whether the relationship is observable or not) is correct, then no examples of eruptive centers fed by dikes or from depth were identified on the north or south flank. Because eruptive centers are often indicators of rifting both on Earth (reviewed by *Walker* [1999]) and in the Tharsis Montes [*Crumpler and Aubele*, 1978], the apparent lack of these centers suggests that Olympus Mons has not begun to develop rift zones along the north or south flank. If the tube-fed flow, raised ridge, and fan units are correctly interpreted as tube-related flows, then their abundance within the map area is ~10%, and the ratio of the channel-fed to tube-related flow units is ~5:1.

[30] Comparison with the Hawaiian shields provides insight into the eruptive and internal dynamics of Olympus Mons. At Hawaii, five Quarternary shield volcanoes show a decrease in lava tube abundance and an increase in the channel-to-tube ratio associated with increased age [*Greeley*, 1987; Bleacher and Greeley, submitted manuscript, 2007]. This transition is related to a change in eruptive dynamics where younger shields experience stable, long-lived eruptions of fluid tholeiitic lavas while older shields experience less stable, shorter-lived eruptions of more viscous and gas-rich alkalic lavas [*Moore and Mark*, 1992; *Wolfe et al.*, 1997; *Rowland and Garbeil*, 2000]. The superposition relationship between the channel-fed and tube-related flow units (Figure 4) indicates that Olympus Mons experienced a similar increase in channel-forming eruptions, resulting in a high channel-to-tube ratio. Although the abundance of lava flow types is related to eruption conditions, those conditions are in turn related to each shield's link to the mantle melt zone. The formation of lava tubes results from high magma production rates which in turn establish long-lived buffered eruptions fed from beneath the magma chamber, whereas a higher ratio of channels to tubes is associated with a decreased rate of magma

production, driving a transition to shorter-lived, unbuffered evacuations of shallow level magma chambers (Bleacher and Greeley, submitted manuscript, 2007).

[31] On the basis of the understanding of the Hawaiian shields the relationship between the Olympus Mons channel-fed and tube-related units, their abundances, and ratio suggests that the late Amazonian surface flows record a cooling mantle source. Crater counts indicate that the distal flow fields are older relative to proximal flow fields as do superposition relationships. These observations are in contradiction to previous mapping that was based on lower resolution images [*Morris and Tanaka*, 1994] but are comparable to trends in lava flow ages at Mauna Loa [*Lockwood and Lipman*, 1987; *Lipman*, 1995; *Lipman and Moore*, 1996]. Therefore we suggest that eruptions at Olympus Mons increasingly produced flows of shorter length (as noted by *Carr et al.* [1977] and *Carr* [1981] for Martian volcanoes) because of a decrease in magma production, which drove the transition from tube- to channel-forming eruptions.

[32] Continued mapping is required to determine if the identified late Amazonian change in eruptive style was limited to specific sectors of Olympus Mons or if it was a volcano-wide phenomenon. *McGovern et al.* [2006] showed that the NE–SW and NW–SE profiles of Olympus Mons are not symmetric, suggesting that differences in tectonic processes might have caused the asymmetry. Lava flow mapping of the entire edifice will show any difference in lava flow emplacement associated with volcano asymmetry. Another question to be addressed is whether the eruptive trend is associated with long-term evolution of the shield and its magma source [*Greeley and Spudis*, 1981] or the waning stage of a more recent episodic cycle [*Wilson et al.*, 2001], both of which have been identified at Hawaii [*Lockwood*, 1995].

[33] The lava flow abundances presented here represent a minimum estimate related to image resolution. The mottled unit is often transitional with the channel-fed and tube-related flow units and is morphologically similar to the surface that comprises the tube-fed flow and raised ridge units. The mottled unit is distributed fairly evenly across the middle flank and also appears to reflect tube-related peaks and troughs in abundance. Therefore the mottled unit might in part represent additional tube-fed flow fields for which younger flows have covered skylights. However, in some cases, MOC images show that the mottled unit is composed of channels that are smaller than the detection limit for the mapping conducted here and/or are significantly covered by dust, supporting the findings of *Malin and Edgett* [2001]. As discussed by *Zimbelman* [2001], data resolution must always be considered when planetary surfaces are interpreted on the basis of remotely sensed data alone. Although MOC images show that the mottled unit might represent lava flow features that are smaller than the detection limit for this study, the combination of HRSC and THEMIS images used for this mapping enable for the first time a consistent estimate of lava flow abundances across Olympus Mons.

6. Conclusions

[34] Mapping lava flow types on Earth provides insight into the eruptive history of shield volcanoes [*Greeley*, 1987; *Holcomb*, 1987; *Lockwood and Lipman*, 1987; *Rowland*, 1996]. Past mapping of Olympus Mons did not consistently differentiate lava flow structures because of image resolution [*Morris and Tanaka*, 1994]. However, new HRSC, THEMIS, and MOC data provide both high-resolution and regional coverage, enabling lava flow types to be differentiated and mapped across a shield. We mapped lava flow types along a north-south transect of Olympus Mons on the basis of HRSC image H0037, in combination with THEMIS and MOC images and MOLA topography data, to determine their abundances and distribution. The resulting map provides new insight into the volcanic history and evolution of the shield during the late Amazonian.

[35] The summit region is typified by a hummocky unit to ~20% distance to the distal margin. The channel-fed flow unit is most abundant between ~20 and 95% of the distance from the caldera. Beyond 95% distance to the distal margin the tabular unit is most common. This transition marks the lower boundary of the basal scarp and a decrease in slope to <2°. No clear structural feature is associated with the transition from the hummocky to channel-fed flow units. We suggest that the hummocky unit is a combination of (1) lava flows lacking well-established tubes or channels, (2) pyroclastic deposits, (3) a dust mantle, and (4) frozen volatiles on the basis of past observations for Olympus Mons and the Hawaiian shields. Unit relationships observed in this study support previous hypotheses that lava fans likely represent local outpourings of lava from within a lava tube. No eruptive centers were identified within this study on the north or south flank, suggesting that no major rift zones have developed in these regions.

[36] The channel-fed to tube-related flow unit ratio (~5:1) and their superposition relationships indicate that Olympus Mons experienced a late Amazonian transition from long-lived, stable, tube-forming eruptions to shorter-lived, less stable, channel-forming eruptions. The same transition is observed at Hawaii, where plate motion extends the distance between the shield and the mantle melt zone, resulting in decreased magma production rates. This suggests that the trends at Olympus Mons, which are likely unrelated to any plate motion, might result from a cooling mantle source. Yet to be determined is whether or not the transition in eruptive dynamics records a long-term evolution of the magma source or the last phase of an episodic cycle, which will be addressed with continued mapping. However, an interesting note is that as magma production rates at older Hawaiian shields approach zero, all lava tubes are covered by channels and pyroclastic deposits, suggesting that the Olympus Mons source region might not yet be extinct.

[37] **Acknowledgments.** We thank the HRSC Experiment Teams at DLR Berlin and Freie Universitaet Berlin as well as the Mars Express Project Teams at ESTEC and ESOC for their successful planning and acquisition of data as well as for making the processed data available to the HRSC Team. We acknowledge the effort of the HRSC Co-Investigator Team members and their associates who have contributed to this investigation in the preparatory phase and in scientific discussions within the team. We also thank R. Beyer and L. Keszthelyi for their thorough and useful reviews of this manuscript. This work is supported by a NASA GSRP grant to J.E.B. and NASA funding to R.G. as a Co-Investigator on the HRSC experiment on Mars Express.

References

Bailey, J. E., A. J. L. Harris, J. Dehn, S. Calvari, and S. K. Rowland (2006), *Bull. Volcanol*, *68*, 497–515.

Bandfield, J. L., V. E. Hamilton, and P. R. Christensen (2000), A global view of Martian surface compositions from MGS-TES, *Science*, *287*, 1626–1630.

Basilevskaya, E. A., G. Neukum, and The HRSC-Co-Investigator Team (2006), The Olympus volcano on Mars: Geometry and characteristics of lava flows, *Sol. Syst. Res.*, *40*(5), 375–383.

Basilevsky, A. T., et al. (2005), Morphology and geological structure of the western part of the Olympus Mons volcano on Mars from the analysis of the Mars Express HRSC imagery, *Sol. Syst. Res.*, *39*(2), 85–101.

Basilevsky, A. T., S. C. Werner, G. Neukum, J. W. Head, S. van Gasselt, K. Gwinner, and B. A. Ivanov (2006), Geologically recent tectonic, volcanic, and fluvial activity on the eastern flank of Olympus Mons volcano, Mars, *Geophys. Res. Lett.*, *33*, L13201, doi:10.1029/2006GL026396.

Burrough, P. A., and R. A. McDonell (1998), *Principles of Geographical Information Systems*, 2nd ed., 356 pp., Oxford Univ. Press, New York.

Calvari, S., and H. Pinkerton (1998), Formation of lava tubes and extensive flow field during the 1991–1993 eruption of Mount Etna, *J. Geophys. Res.*, *103*, 27,291–27,301.

Calvari, S., and H. Pinkerton (1999), Lava tube morphology on Etna and evidence for lava flow emplacement mechanism, *J. Volcanol. Geotherm. Res.*, *90*, 263–280.

Calvari, S., M. Neri, and H. Pinkerton (2003), Effusion rate estimations during the 1999 summit eruption on Mount Etna, and growth of two distinct lava flow fields, *J. Volcanol. Geotherm. Res.*, *119*, 107–123.

Carr, M. H. (1973), Volcanism on Mars, *J. Geophys. Res.*, *78*, 4049–4062.

Carr, M. H. (1981), *The Surface of Mars*, 232 pp., Yale Univ. Press, New Haven, Conn.

Carr, M. H., and R. Greeley (1980), Volcanic features of Hawaii: A basis for comparison with Mars, *NASA Spec. Publ., SP-403*, 211 pp.

Carr, M. H., R. Greeley, K. R. Blasius, J. E. Guest, and J. B. Murray (1977), Some Martian volcanic features as viewed from the Viking orbiters, *J. Geophys. Res.*, *82*, 3985–4015.

Christensen, P. R., et al. (2004), The Thermal Emission Imaging System (THEMIS) for the Mars 2001 Odyssey Mission, *Space Sci. Rev.*, *110*, 85–130.

Crumpler, L. S., and J. C. Aubele (1978), Structural evolution of Arsia Mons, Pavonis Mons, and Ascraeus Mons: Tharsis region of Mars, *Icarus*, *34*, 496–511.

Edgett, K. S. (1997), Aeolian dunes as evidence for explosive volcanism in the Tharsis region of Mars, *Icarus*, *130*, 96–114.

Edgett, K. S., and M. C. Malin (2002), Martian sedimentary rock statrigraphy: Outcrops and interbedded craters of northwest Sinus Meridiani and southwest Arabia Terra, *Geophys. Res. Lett.*, *29*(24), 2179, doi:10.1029/2002GL016515.

Edgett, K. S., B. J. Butler, J. R. Zimbelman, and V. E. Hamilton (1997), Geologic context of the Mars radar "Stealth" region in southwestern Tharsis, *J. Geophys. Res.*, *102*, 21,545–21,567.

Greeley, R. (1973), Mariner 9 photographs of small volcanic structures on Mars, *Geology*, *1*, 175–180.

Greeley, R. (1977), Volcanic morphology, in *Volcanism of the Eastern Snake River Plain, Idaho: A Comparative Planetary Geology Guidebook*, edited by R. Greeley and J. S. King, *NASA CR-154621,* pp. 5–22, NASA, Washington, D. C.

Greeley, R. (1987), The role of lava tubes in Hawaiian volcanoes, in *Volcanism in Hawaii*, edited by R. W. Decker et al., *U.S. Geol. Surv. Prof. Pap., 1350*, 1589–1605.

Greeley, R., and D. E. Gault (1979), Endogenic craters on basaltic lava flows: Size frequency distributions, *Proc. Lunar Planet. Sci. Conf.*, *10th*, 2919–2933.

Greeley, R., and J. Iversen (1985), *Wind as a Geological Process on Earth, Mars, Venus, and Titan*, 348 pp., Cambridge Univ. Press, New York.

Greeley, R., and P. D. Spudis (1981), Volcanism on Mars, *Rev. Geophys.*, *19*, 13–41.

Gregg, T. K. P., and J. H. Fink (2000), A laboratory investigation into the effects of slope on lava flow morphology, *J. Volcanol. Geotherm. Res.*, *96*, 145–159.

Guest, J. E., C. R. J. Kilburn, H. Pinkerton, and A. M. Duncan (1987), The evolution of lava flow-fields: Observations of the 1981 and 1983 eruptions of Mount Etna, Sicily, *Bull. Volcanol.*, *49*, 527–540.

Hartmann, W. K. (2005), Martian cratering 8: Isochron refinement and the chronology of Mars, *Icarus*, *174*, 294–320.

Hartmann, W. K., and G. Neukum (2001), Cratering chronology and evolution of Mars, *Space Sci. Rev.*, *96*, 165–194.

Hartmann, W. K., et al. (1981), Chronology of planetary volcanism by comparative studies of planetary cratering, in *Basaltic Volcanism on the Terrestrial Planets*, edited by W. M. Kaula et al., pp. 1049–1127, Elsevier, New York.

Head, J. W., W. B. Bryan, R. Greeley, J. E. Guest, P. H. Shultz, R. S. J. Sparks, G. P. L. Walker, J. L. Whitford-Stark, C. A. Wood, and M. H. Carr (1981), Distribution and morphology of basalt deposits on planets, in *Basaltic Volcanism on the Terrestrial Planets*, edited by W. M. Kaula et al., pp. 702–887, Elsevier, New York.

Heliker, C. C., M. T. Mangan, T. N. Mattox, J. P. Kauahikaua, and R. T. Helz (1998), The character of long-term eruptions: Inferences from episodes 50–53 of the Puu Oo-Kupaianaha eruption of Kilauea Volcano, *Bull. Volcanol.*, *59*, 381–393.

Holcomb, R. T. (1987), Eruptive history and long-term behavior of Kilauea Volcano, in *Volcanism in Hawaii*, edited by R. W. Decker et al., *U.S. Geol. Surv. Prof. Pap., 1350*, 261–350.

Holcomb, R. T., D. W. Peterson, and R. I. Tilling (1974), Recent landforms at Kilauea volcano: A selected photographic compilation, in *Geologic Guide to the Island of Hawaii: A Field Guide for Comparative Planetary Geology*, edited by R. Greeley, *NASA CR-152416*, pp. 49–86, NASA, Washington, D. C.

Kauahikaua, J., K. V. Cashman, T. N. Mattox, C. C. Heliker, K. A. Hon, M. T. Mangan, and C. R. Thornber (1998), Observations on basaltic lava streams in tubes from Kilauea volcano, Island of Hawaii, *J. Geophys. Res.*, *103*, 27,303–27,323.

Kauahikaua, J., D. R. Sherrod, K. V. Cashman, C. Heliker, K. Hon, T. N. Mattox, and J. A. Johnson (2003), Hawaiian lava-flow dynamics during the Puu Oo-Kupaianaha eruption: A tale of two decades, in *The Puu Oo-Kupaianaha Eruption of Kilauea Volcano, Hawaii, the First 20 Years*, edited by C. Heliker et al., *U.S. Geol. Surv. Prof. Pap., 1676*, 63–87.

Keszthelyi, L. (1995), A preliminary thermal budget for lava tubes on the Earth and planets, *J. Geophys. Res.*, *100*, 20,411–20,420.

Kilburn, C. R. J., and R. M. C. Lopes (1991), General patterns of flow field growth: Aa and blocky lavas, *J. Geophys. Res.*, *96*, 19,721–19,732.

Kreslavsky, M. A., and J. W. Head III (1999), Kilometer-scale slopes on Mars and their correlation with geologic units: Initial results from Mars Orbiter Laser Altimeter (MOLA) data, *J. Geophys. Res.*, *104*, 21,911–21,924.

Kreslavsky, M. A., and J. W. Head III (2000), Kilometer-scale roughness of Mars: Results from MOLA data analysis, *J. Geophys. Res.*, *105*, 26,695–26,711.

Lipman, P. W. (1995), Declining growth of Mauna Loa volcano during the last 100000 years: Rates of lava accumulation vs. gravitational subsidence, in *Mauna Loa Revealed: Structure, Composition, History, and Hazards*, *Geophys. Monogr. Ser.*, vol. 92, edited by J. M. Rhodes and J. P. Lockwood, pp. 45–80, AGU, Washington, D. C.

Lipman, P. W., and J. G. Moore (1996), Mauna Loa lava accumulation rates at the Hilo drill site: Formation of lava deltas during a period of declining overall volcanic growth, *J. Geophys. Res.*, *101*, 11,631–11,641.

Lockwood, J. P. (1995), Mauna Loa eruptive history—The preliminary radiocarbon record, in *Mauna Loa Revealed: Structure, Composition, History, and Hazards*, *Geophys. Monogr. Ser.*, vol. 92, edited by J. M. Rhodes and J. P. Lockwood, pp. 81–94, AGU, Washington, D. C.

Lockwood, J. P., and P. W. Lipman (1987), Holocene eruptive history of Mauna Loa Volcano, in *Volcanism in Hawaii*, edited by R. W. Decker et al., *U.S. Geol. Surv. Prof. Pap., 1350*, 509–536.

Longley, P. A., M. F. Goodchild, D. J. Maguire, and D. W. Rhind (2001), *Geographic Information Systems and Science*, 454 pp., John Wiley, Hoboken, N. J.

Macdonald, G. A. (1956), Pahoehoe, aa, and block lava, *Am. J. Sci.*, *251*, 169–191.

Malin, M. C., and K. S. Edgett (2001), Mars Global Surveyor Mars Orbiter Camera: Interplanetary cruise through the primary mission, *J. Geophys. Res.*, *106*, 23,429–23,570.

Malin, M. C., G. E. Danielson, A. P. Ingersoll, H. Masursky, J. Veverka, M. A. Ravine, and T. A. Soulanille (1992), Mars Observer Camera, *J. Geophys. Res.*, *97*, 7699–7718.

McCauley, J. F., M. H. Carr, J. A. Cutts, W. K. Hartmann, H. Masursky, D. J. Milton, R. P. Sharp, and D. E. Wilhelms (1972), Preliminary Mariner 9 report on the geology of Mars, *Icarus*, *17*, 289–327.

McEwen, A. S., B. S. Preblich, E. P. Turtle, N. A. Artemieva, M. P. Golombek, M. Hurst, R. L. Kirk, D. M. Burr, and P. R. Christensen (2005), The rayed crater Zunil and interpretations of small impact craters on Mars, *Icarus*, *176*, 351–381.

McGovern, P. J., and S. C. Solomon (1993), State of stress, faulting, and eruption characteristics of large volcanoes on Mars, *J. Geophys. Res.*, *98*, 23,553–23,579.

McGovern, P. J., J. R. Smith, J. K. Morgan, and M. H. Bulmer (2004), Olympus Mons aureole deposits: New evidence for a flank failure origin, *J. Geophys. Res.*, *109*, E08008, doi:10.1029/2004JE002258.

McGovern, P. J., J. K. Morgan, and M. A. Higbie (2006), Structure and evolution of the Olympus Mons volcanic edifice and basal escarpment, Mars, *Lunar Planet. Sci.*, [CD-ROM], XXXVII, Abstract 2329.

Mellon, M. T., B. M. Jakosky, H. H. Kieffer, and P. R. Christensen (2000), High-resolution thermal intertia mapping from the Mars Global Surveyor Thermal Emission Spectrometer, *Icarus*, *148*, 437–455.

Moore, J. G., and R. K. Mark (1992), Morphology of the Island of Hawaii, *GSA Today*, *2*(11), 257–262.

Morris, E. C., and K. L. Tanaka (1994), Geologic maps of the Olympus Mons region of Mars, *U.S. Geol. Surv. Misc. Invest. Ser. Map, I-2327*, scale 1:2,000,000 and 1:1,000,000.

Mouginis-Mark, P. J. (2002), Prodigious ash deposits near the summit of Arsia Mons volcano, Mars, *Geophys. Res. Lett.*, *29*(16), 1768, doi:10.1029/2002GL015296.

Mouginis-Mark, P. J., and P. R. Christensen (2005), New observations of volcanic features on Mars from the THEMIS instrument, *J. Geophys. Res.*, *110*, E08007, doi:10.1029/2005JE002421.

Mouginis-Mark, P. J., L. Wilson, and M. T. Zuber (1992), The physical volcanology of Mars, in *Mars*, edited by H. H. Kieffer et al., pp. 424–452, Univ. of Ariz. Press, Tucson.

Neukum, G., R. Jaumann, and the HRSC Co-Investigator and Experiment Team (2004a), HRSC: The High Resolution Stereo Camera of Mars Express, in *Mars Express: The Scientific Payload*, edited by A. Wilson, *Eur. Space Agency Spec. Publ., ESA SP-1240*, 17–36.

Neukum, G., et al. (2004b), Recent, episodic volcanic and glacial activity on Mars revealed by the High Resolution Stereo Camera, *Nature*, *432*, 971–979.

Peterson, D. W., R. T. Holcomb, R. I. Tilling, and R. L. Chirstiansen (1994), Development of lava tubes in the light of observations at Mauna Ulu, Kilauea volcano, Hawaii, *Bull Volcanol.*, *56*, 343–360.

Plescia, J. B. (2004), Morphometric properties of Martian volcanoes, *J. Geophys. Res.*, *109*, E03003, doi:10.1029/2002JE002031.

Plescia, J. B. (2005), Small-diameter Martian craters: Applicability for chronology, *Lunar Planet. Sci.*, [CD-ROM], XXXVI, Abstract 2171.

Plescia, J. B., and R. S. Saunders (1979), The chronology of the Martian volcanoes, in *Proc. Lunar Planet. Sci. Conf.*, 10th, 2841–2859.

Pupysheva, N. V., A. T. Basilevsky, and B. A. Ivanov (2006), Lava tubes on the summit part of Olympus Mons volcano, Mars, and channel network at its south-east foot: Morphology, depths, widths, lengths, and coefficients of sinuosity, paper presented at 44th Vernadsky-Brown Microsymposium on Comparative Planetology, Moscow, 9–11 Oct.

Rowland, S. K. (1996), Slopes, lava flow volumes, and vent distributions on Volcan Fernandina, Galapagos Islands, *J. Geophys. Res.*, *101*, 27,657–27,672.

Rowland, S. K., and H. Garbeil (2000), Slopes of oceanic basalt volcanoes, in *Remote Sensing of Active Volcanism*, *Geophys. Monogr. Ser.*, vol. 116, edited by P. J. Mouginis-Mark et al., pp. 223–248, AGU, Washington, D. C.

Rowland, S. K., and G. P. L. Walker (1990), Pahoehoe and aa in Hawaii: Volumetric flow rate controls the lava structure, *Bull. Volcanol.*, *52*, 615–628.

Sakimoto, S. E. H., and M. T. Zuber (1998), Flow and convection cooling in lava tubes, *J. Geophys. Res.*, *103*, 27,465–27,487.

Scott, D. H., and M. H. Carr (1978), Geologic map of Mars, *U.S. Geol. Surv. Misc. Invest. Ser. Map, I-1083*, scale 1:25,000,000.

Scott, D. H., and K. L. Tanaka (1981a), Map showing lava flows in the northeast part of the Amazonis Quadrangle of Mars, *U.S. Geol. Surv. Misc. Invest. Ser. Map, I-1279*, scale 1:2,000,000.

Scott, D. H., and K. L. Tanaka (1981b), Map showing lava flows in the southeast part of the Amazonis Quadrangle of Mars, *U.S. Geol. Surv. Misc. Invest. Ser. Map, I-1280,* scale 1:2,000,000.

Scott, D. H., and K. L. Tanaka (1986), Geologic map of the western equatorial region of Mars, *U.S. Geol. Surv. Misc. Invest. Ser. Map, I-1802-A*, scale 1:15000000.

Scott, D. H., G. G. Schaber, K. C. Horstman, A. L. Dial Jr., and K. L. Tanaka (1981a), Map showing lava flows in the northwest part of the Tharsis Quadrangle of Mars, *U.S. Geol. Surv. Misc. Invest. Ser. Map, I-1266*, scale 1:2,000000.

Scott, D. H., G. G. Schaber, K. C. Horstman, A. L. Dial Jr., and K. L. Tanaka (1981b), Map showing lava flows in the southwest part of the Tharsis Quadrangle of Mars, *U.S. Geol. Surv. Misc. Invest. Ser. Map, I-1268*, scale 1:2,000000.

Smith, D. E., et al. (1999), The global topography of Mars and implications for surface evolution, *Science*, *284*, 1495–1503.

Smith, D. E., et al. (2001), Mars Orbiter Laser Altimeter: Experiment summary after the first year of global mapping of Mars, *J. Geophys. Res.*, *106*, 23,689–23,722.

Smith, D., G. Neumann, R. E. Arvidson, E. A. Guinness, and S. Slavney (2003), Mars Global Surveyor Laser Altimeter Mission Experiment Gridded Data Record, MGS-M-MOLA-5-MEGDR-L3-V1.0, http://pds-geosciences.wustl.edu/, NASA Planet. Data Syst. St. Louis, Mo.

Swanson, D. A. (1973), Pahoehoe flows from the 1969–1971 Mauna Ulu eruption, Kilauea volcano, Hawaii, *Geol. Soc. Am. Bull.*, *84*, 615–626.

Thomas, P. J., S. W. Squyres, and M. H. Carr (1990), Flank tectonics of Martian volcanoes, *J. Geophys. Res.*, *95*, 14,345–14,355.

Walker, G. P. L. (1999), Volcanic rift zones and their intrusion swarms, *J. Volcanol. Geotherm. Res.*, *94*, 21–34.

Wentworth, C. K., and G. A. Macdonald (1953), Structures and forms of basaltic rocks in Hawaii, *U.S. Geol. Surv. Bull.*, *994*, 1–90.

Werner, S. (2005), Major aspects of the chronostratigraphy and geologic evolutionary history of Mars, Ph.D. dissertation, Free Univ., Berlin. (Available at http://www.diss.fu-berlin.de/2006/33/index.html)

Whitford-Stark, J. L. (1982), Factors influencing the morphology of volcanic landforms: An Earth-Moon comparison, *Earth Sci. Rev.*, *18*, 109–168.

Wilson, L., E. D. Scott, and J. W. Head (2001), Evidence for episodicity in the magma supply to the large Tharsis volcanoes, *J. Geophys. Res.*, *106*, 1423–1433.

Wolfe, E. W., W. S. Wise, and G. B. Dalrymple (1997), The geology and petrology of Mauna Kea volcano, Hawaii—A study of postshield volcanism, *U.S. Geol. Surv. Prof. Pap., 1557*, 129 pp.

Zimbelman, J. R. (2001), Image resolution and the evaluation of genetic hypotheses for planetary landscapes, *Geomorphology*, *37*, 179–199.

J. E. Bleacher, Planetary and Geodynamics Laboratory, NASA GSFC, Code 698, Building 33, Room G310, Greenbelt, MD 20771, USA. (jake@puuoo.gsfc.nasa.gov)

R. Greeley and D. A. Williams, School of Earth and Space Exploration, Arizona State University, Tempe, AZ 85287, USA.

E. Hauber, Institute of Planetary Research, DLR, Leitung und Infrastruktur Rutherfordstraβe 2, D-12489 Berlin, Germany.

G. Neukum and S. C. Werner, Institute of Geological Sciences, Freie Universitaet, Malteserstrasse 74-100, D-12249 Berlin, Germany.